In situ three-dimensional monitoring of collagen fibrillogenesis using SHG microscopy

S. Bancelin,[1] C. Aimé,[2] T. Coradin,[2] and M.-C. Schanne-Klein[1,*]

[1]*Ecole Polytechnique; CNRS; INSERM U696, Laboratoire d'Optique et Biosciences, F-91128 Palaiseau, France*
[2]*UPMC Univ Paris 06; CNRS, Chimie de la Matière Condensée de Paris, Collège de France, 11 place Marcelin Berthelot, F-75005 Paris, France*
**marie-claire.schanne.klein@polytechnique.edu*

Abstract: We implemented *in situ* time-lapse Second Harmonic Generation (SHG) microscopy to monitor the three-dimensional (3D) self-assembly of collagen in solution. As a proof of concept, we tuned the kinetics of fibril formation by varying the pH and measured the subsequent exponential increase of fibril volume density in SHG images. We obtained significantly different time constants at pH = 6.5 ± 0.3 and at pH = 7.5 ± 0.3. Moreover, we showed that we could focus on the growth of a single isolated collagen fibril because SHG microscopy is sensitive to well-organized fibrils with diameter below the optical resolution. This work illustrates the potential of SHG microscopy for the rational design and characterization of collagen-based biomaterials.

OCIS codes: (180.4315) Nonlinear microscopy; (180.6900) Three-dimensional microscopy; (190.2620) Harmonic generation and mixing; (170.6935) Tissue characterization; (190.4180) Multiphoton processes; (190.4710) Optical nonlinearities in organic materials.

References and links

1. D. E. Birk and P. Bruckner, "Collagen suprastructures," Top. Curr. Chem. **247**, 185–205 (2005).
2. M.-M. Giraud-Guille, L. Besseau, and R. Martin, "Liquid crystalline assemblies of collagen in bone and *in vitro* systems," J. Biomech. **36**(10), 1571–1579 (2003).
3. S. Köster, H. M. Evans, J. Y. Wong, and T. Pfohl, "An *in situ* study of collagen self-assembly processes," Biomacromolecules **9**(1), 199–207 (2008).
4. C. B. Raub, V. Suresh, T. Krasieva, J. Lyubovitsky, J. D. Mih, A. J. Putnam, B. J. Tromberg, and S. C. George, "Noninvasive assessment of collagen gel microstructure and mechanics using multiphoton microscopy," Biophys. J. **92**(6), 2212–2222 (2007).
5. J. R. Harris and A. Reiber, "Influence of saline and pH on collagen type I fibrillogenesis *in vitro*: fibril polymorphism and colloidal gold labelling," Micron **38**(5), 513–521 (2007).
6. F. Gobeaux, G. Mosser, A. Anglo, P. Panine, P. Davidson, M.-M. Giraud-Guille, and E. Belamie, "Fibrillogenesis in dense collagen solutions: a physicochemical study," J. Mol. Biol. **376**(5), 1509–1522 (2008).
7. F. Z. Jiang, H. Hörber, J. Howard, and D. J. Müller, "Assembly of collagen into microribbons: effects of pH and electrolytes," J. Struct. Biol. **148**(3), 268–278 (2004).
8. T. Starborg, Y. Lu, K. E. Kadler, and D. F. Holmes, "Electron microscopy of collagen fibril—structure *in vitro* and *in vivo* including three-dimensional reconstruction," in *Methods in Cell Biology* (Elsevier, 2008), Vol. 88, 319–345.
9. V. K. Yadavalli, D. V. Svintradze, and R. M. Pidaparti, "Nanoscale measurements of the assembly of collagen to fibrils," Int. J. Biol. Macromol. **46**(4), 458–464 (2010).
10. D. A. Cisneros, C. Hung, C. M. Franz, and D. J. Muller, "Observing growth steps of collagen self-assembly by time-lapse high-resolution atomic force microscopy," J. Struct. Biol. **154**(3), 232–245 (2006).
11. A. O. Brightman, B. P. Rajwa, J. E. Sturgis, M. E. McCallister, J. P. Robinson, and S. L. Voytik-Harbin, "Time-lapse confocal reflection microscopy of collagen fibrillogenesis and extracellular matrix assembly *in vitro*," Biopolymers **54**(3), 222–234 (2000).
12. Y. L. Yang and L. J. Kaufman, "Rheology and confocal reflectance microscopy as probes of mechanical properties and structure during collagen and collagen/hyaluronan self-assembly," Biophys. J. **96**(4), 1566–1585 (2009).
13. K. Wolf, S. Alexander, V. Schacht, L. M. Coussens, U. H. von Andrian, J. van Rheenen, E. Deryugina, and P. Friedl, "Collagen-based cell migration models *in vitro* and *in vivo*," Semin. Cell Dev. Biol. **20**(8), 931–941 (2009).
14. I. Freund and M. Deutsch, "Second-harmonic microscopy of biological tissue," Opt. Lett. **11**(2), 94–96 (1986).

#166900 - $15.00 USD Received 18 Apr 2012; revised 16 May 2012; accepted 16 May 2012; published 21 May 2012

15. P. J. Campagnola, A. C. Millard, M. Terasaki, P. E. Hoppe, C. J. Malone, and W. A. Mohler, "Three-dimensional high-resolution second-harmonic generation imaging of endogenous structural proteins in biological tissues," Biophys. J. **82**(1), 493–508 (2002).
16. A. Zoumi, A. Yeh, and B. J. Tromberg, "Imaging cells and extracellular matrix *in vivo* by using second-harmonic generation and two-photon excited fluorescence," Proc. Natl. Acad. Sci. U.S.A. **99**(17), 11014–11019 (2002).
17. W. R. Zipfel, R. M. Williams, R. Christie, A. Y. Nikitin, B. T. Hyman, and W. W. Webb, "Live tissue intrinsic emission microscopy using multiphoton-excited native fluorescence and second harmonic generation," Proc. Natl. Acad. Sci. U.S.A. **100**(12), 7075–7080 (2003).
18. M. Strupler, A.-M. Pena, M. Hernest, P.-L. Tharaux, J.-L. Martin, E. Beaurepaire, and M.-C. Schanne-Klein, "Second harmonic imaging and scoring of collagen in fibrotic tissues," Opt. Express **15**(7), 4054–4065 (2007).
19. R. W. Boyd, *Nonlinear Optics* (Academic, 2003).
20. S. V. Plotnikov, A. C. Millard, P. J. Campagnola, and W. A. Mohler, "Characterization of the myosin-based source for second-harmonic generation from muscle sarcomeres," Biophys. J. **90**(2), 693–703 (2006).
21. A. Deniset-Besseau, J. Duboisset, E. Benichou, F. Hache, P.-F. Brevet, and M.-C. Schanne-Klein, "Measurement of the second-order hyperpolarizability of the collagen triple helix and determination of its physical origin," J. Phys. Chem. B **113**(40), 13437–13445 (2009).
22. A. Deniset-Besseau, P. De Sa Peixoto, G. Mosser, and M.-C. Schanne-Klein, "Nonlinear optical imaging of lyotropic cholesteric liquid crystals," Opt. Express **18**(2), 1113–1121 (2010).
23. A.-M. Pena, T. Boulesteix, T. Dartigalongue, and M.-C. Schanne-Klein, "Chiroptical effects in the second harmonic signal of collagens I and IV," J. Am. Chem. Soc. **127**(29), 10314–10322 (2005).
24. C. Bayan, J. M. Levitt, E. Miller, D. Kaplan, and I. Georgakoudi, "Fully automated, quantitative, noninvasive assessment of collagen fiber content and organization in thick collagen gels," J. Appl. Phys. **105**(10), 102042 (2009).
25. A.-M. Pena, D. Fagot, C. Olive, J.-F. Michelet, J.-B. Galey, F. Leroy, E. Beaurepaire, J.-L. Martin, A. Colonna, and M.-C. Schanne-Klein, "Multiphoton microscopy of engineered dermal substitutes: assessment of 3-D collagen matrix remodeling induced by fibroblast contraction," J. Biomed. Opt. **15**(5), 056018 (2010).
26. M.-M. Giraud-Guille, L. Besseau, D. Herbage, and P. Gounon, "Optimization of Collagen Liquid-Crystalline Assemblies - Influence of Sonic Fragmentation," J. Struct. Biol. **113**(2), 99–106 (1994).
27. I. Gusachenko, V. Tran, Y. G. Houssen, J.-M. Allain, and M.-C. Schanne-Klein, "Polarization-resolved second-harmonic microscopy in tendon upon mechanical stretching," Biophys. J. **102**(9), 2220–2229 (2012).
28. G. Latour, I. Gusachenko, L. Kowalczuk, I. Lamarre, and M.-C. Schanne-Klein, "*In vivo* structural imaging of the cornea by polarization-resolved second harmonic microscopy," Biomed. Opt. Express **3**(1), 1–15 (2012).
29. M.-M. Giraud Guille, C. Helary, S. Vigier, and N. Nassif, "Dense fibrillar collagen matrices for tissue repair," Soft Matter **6**(20), 4963–4967 (2010).

1. Introduction

Type I collagen is a ubiquitous protein that is the main constituent of connective tissues. Synthesized by cells as triple helix units, collagen self-assembles into fibrils *in vivo* and *in vitro* forming three-dimensional (3D) networks [1–3]. This assembly mechanism depends critically on the collagen concentration, as well as on the temperature, pH and ionic strength of the solution [4–7]. To get insight into the molecular mechanisms of collagen assembly, transmission electron microscopy (TEM) is routinely used at different stages to obtain highly resolved images at the nanometer scale [8]. The structure of collagen fibrils and the kinetics of fibrillogenesis have also been investigated using atomic force microscopy [9,10] which enables *in situ* imaging in liquid solutions. However, there is a need for non-invasive 3D imaging techniques to monitor and quantify collagen assembly in a 3D environment. In this regard, optical techniques such as confocal reflectance microscopy [11–13] and Second Harmonic Generation (SHG) microscopy [13–18] appear as powerful techniques to visualize the 3D architecture of collagen networks in biological tissues without any labeling. However, one main disadvantage of confocal microscopy is that reflectance signals are intrinsically non-specific.

In this paper, we focus on SHG microscopy, which is a multiphoton imaging technique complementary to two-photon excited fluorescence (2PEF) microscopy. As such, it is characterized by intrinsic optical sectioning and provides improved depth penetration in scattering tissues with sub-micrometer resolution. SHG is a coherent multiphoton process, which radiates at exactly half the excitation wavelength [19], and is highly specific for dense non-centrosymmetric media [14–18]. At the molecular level, SHG originates from the presence of polarizable electrons with a non-centrosymmetric environment in peptide bonds [20,21]. At the macromolecular level, SHG is obtained as the coherent summation of the

#166900 - $15.00 USD Received 18 Apr 2012; revised 16 May 2012; accepted 16 May 2012; published 21 May 2012

harmonic fields radiated by all the peptide bonds within the focal volume. SHG radiation is coherently amplified in highly anisotropic fibrillar collagen because of the tight alignment of peptide bonds along the collagen triple helix and within fibrils [21]. Accordingly, type I fibrillar collagen exhibits strong endogenous SHG signals without the addition of exogenous labels. This SHG signal scales quadratically with the number of aligned molecules, which results in highly contrasted images [22]. On the contrary, type IV non-fibrillar collagen, which is organized as a loose centrosymmetrical network in basal membranes, does not exhibit any SHG signal because of destructive interferences [18,23]. SHG microscopy is therefore considered as a sensitive structural probe of the macromolecular organization of collagen.

While SHG microscopy has been used in recent years to characterize the architecture of collagen fibrils in collagen matrices [4,16,24,25], the kinetics of fibrillogenesis has not been investigated using this technique. In this work, we report 3D *in situ* time-lapse SHG imaging of collagen fibrillogenesis in diluted solution ([collagen] = 100 µg/ml), at a constant room temperature. We show that SHG provides reliable 3D quantitative information on fibril formation. Importantly, we show for the first time that SHG can be used to monitor the growth of a single isolated collagen fibril in solution, with diameter below the optical resolution.

2. Materials and methods

2.1. Sample preparation

Type I collagen was extracted and purified from rat tail tendons as previously described [6,26]. All other chemicals were purchased and used as received. Water was purified with a Direct-Q system (Millipore Co.). Collagen (100 µg/ml) was solubilized in 0.5 M acetic acid and fibrillogenesis was triggered upon increasing pH to 6.5 ± 0.3 and 7.5 ± 0.3 by addition of NaOH, in order to tune the kinetics of fibrillogenesis. Because temperature is known to impact both fibrillogenesis kinetics and fibril diameter, we kept the temperature constant at 21° C ± 0.5°. A drop of sample was placed between two glass coverslips and directly visualized using SHG microscopy without any staining.

2.2. SHG microscopy

Multiphoton imaging was performed using a custom-built laser scanning microscope [18,22], based on a femtosecond Ti:sapphire laser (Tsunami, Spectra-Physics). Samples were illuminated in an upright geometry using circularly-polarized excitation at 860 nm (ellipticity 0.88) to enable homogenous imaging of fibrils whatever their orientation in the focal plane. SHG signals were recorded in photon-counting photomultiplier tubes (P25PC, Electron Tubes) using appropriate dichroic mirror and spectral filters (FF01-680/SP, FF01-720/SP and FF01-427/10, Semrock). High numerical aperture water immersion objective (40×, NA 1.10, LD C-Apochromat, Zeiss) was used to achieve typical lateral and axial resolutions of 0.36 × 1.2 μm^2 at 860 nm excitation. SHG image stacks were recorded in forward direction using 100 kHz pixel rate with 0.27 µm pixel size, 0.5 µm axial steps and 55 mW typical laser power at the objective focus. Typical size of image stacks is 163 × 159 × 30 μm^3 (corresponding to 600 × 590 × 60 voxels). Stacks of SHG images were recorded in about five minutes in these conditions. Sequential acquisitions were performed every ten to twenty minutes for rapid and slow kinetics respectively.

2.3. Image processing

SHG images were analyzed using ImageJ software (W. Rasband, NIH). Background in the SHG images was quite low once the laser excitation was properly filtered out using laser blocking emission filters and the SHG was properly selected using ~10 nm wide bandpass filters (see above). However, the surface area of this nonsignificant background may not be negligible compared to the SHG signal from sparse collagen fibrils in a diluted sample. It was therefore filtered out using a median filter (1.0 pixel radius). Stacks were then projected along

#166900 - $15.00 USD Received 18 Apr 2012; revised 16 May 2012; accepted 16 May 2012; published 21 May 2012

z-axis and the extent of the fibrillar network was quantified by calculating the area fraction of pixels with SHG signal [4,18,24,25]. No threshold was applied at this stage since the median filter efficiently removed nonsignificant SHG background.

2.4 Transmission electron microscopy

A small drop of sample in aqueous solution was deposited on carbon-coated copper grids (300 mesh) without any staining. After 3 minutes, the excess liquid was blotted with filter paper (Whatman #4). Observations were performed at room temperature using a JEOL 1011 electron microscope operating at 100 kV and the images were recorded on a Gatan Orius CCD camera.

3. Results

3.1. In situ 3D visualization of fibrillogenesis

Modification of temperature, ionic strength and pH has a critical effect on collagen fibrillogenesis [4–7]. In particular, decreasing pH slightly above neutral value slows down the kinetics of fibril formation due to electrostatic repulsion between collagen triple helices. As a proof of concept, we performed time-lapse SHG imaging to investigate collagen fibrillogenesis at two different pH, *i.e.* following two different kinetic regimes. Fibrillogenesis has been triggered by adjusting the pH to 6.5 ± 0.3 for samples referred hereafter as "*slow* kinetic samples," with respect to samples having a pH of 7.5 ± 0.3 so called "*fast* kinetic samples." These two conditions aimed at underlying the reliability and the different kinetics accessible with such a technique.

For each kinetic, four independent samples have been investigated, where fibrils density increased over time before reaching a plateau. This is illustrated in Fig. 1, which displays 3D reconstructions of the fibrils density during collagen fibrillogenesis at six different times. In this case (pH = 6.5 ± 0.3), the plateau is reached after about 490 minutes.

The background noise is quite important in the first SHG reconstruction in Fig. 1 (recorded after 30 min), even after image processing. This background mainly results from electronic noise in the amplification stage of the photomultiplier tube (PMT) that accumulates during sample setting with light on. However, the PMT spontaneously discharges in the dark,

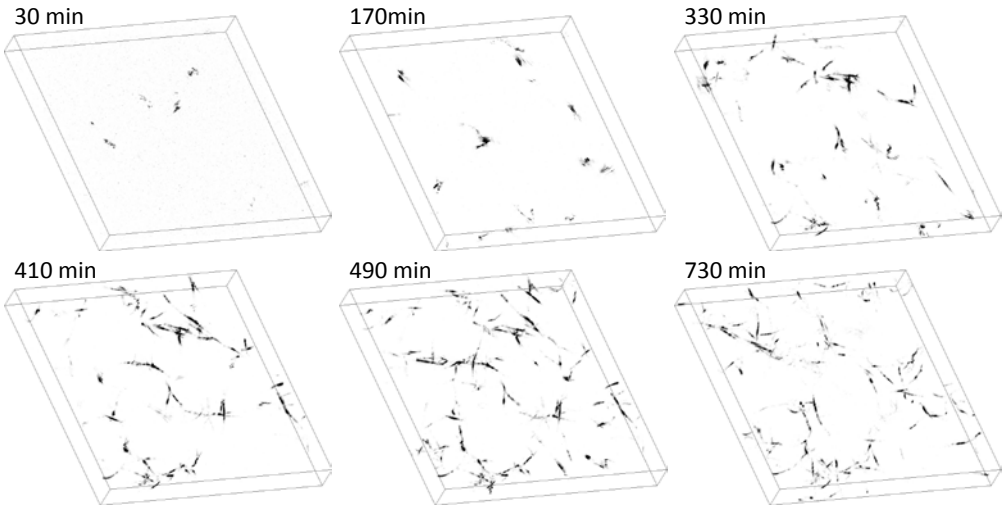

Fig. 1. 3D reconstruction of SHG images of collagen fibrillogenesis in a slow kinetic sample (pH = 6.5 ± 0.3). Acquisition times are indicated in top of every image. Image size: 163 × 159 × 30 μm^3.

#166900 - $15.00 USD Received 18 Apr 2012; revised 16 May 2012; accepted 16 May 2012; published 21 May 2012

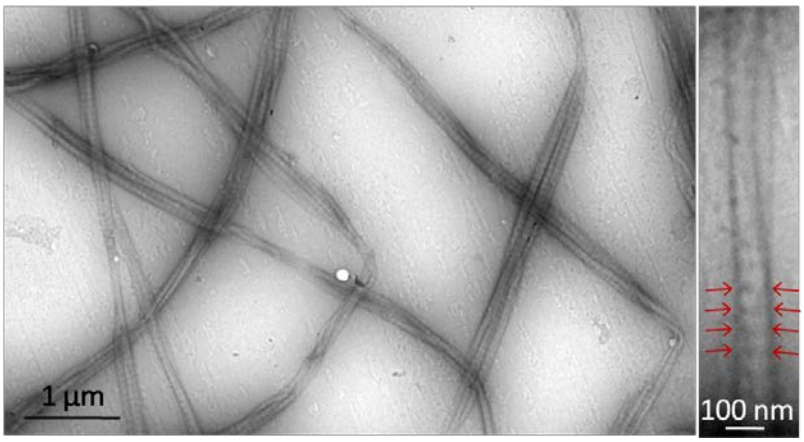

Fig. 2. TEM micrographs of collagen fibrils observed in a slow kinetic sample (pH = 6.5 ± 0.3), at different magnifications. Red arrows underline the characteristic D-banded periodicity.

so that this background noise rapidly decreases and becomes negligible after 20 minutes for the following acquisition.

In parallel, TEM observations performed on slow kinetics samples evidenced the formation of collagen fibrils having the typical expected structure. In particular, these fibrils exhibited the characteristic D-banded periodicity of about 67 nm, observed in all collagen tissues *in vivo* [1,2,5,6,8] (Fig. 2, red arrows).

3.2. Kinetics of fibrillogenesis

We used a statistical approach to quantitatively analyze these SHG images and calculate the volume density of fibrils within each sample during fibrillogenesis. Figures 3(a) and 3(b) display the evolution of fibril density in two samples at pH = 6.5 ± 0.3 and pH = 7.5 ± 0.3 respectively. These experimental data were fitted with an exponential function,

$$y(t) = \frac{\tau}{B}\left(1 - e^{-\frac{t}{\tau}}\right),$$

to obtain the fibrillogenesis exponential time constants τ displayed in Table 1. Exponential fitting was less accurate for fast kinetics samples (see Fig. 3(b)) than for slow kinetics ones (see Fig. 3(a)) because of the limited number of experimental data that could be acquired during a fast fibrillogenesis. We also often observed a first small peak before the plateau, which decrease is presumably due to slight sedimentation of the collagen fibrils within the solution. Nevertheless, the data from all samples were satisfactorily fitted using exponential functions.

It is worth noting that, as an off-resonance technique, SHG microscopy provides a non-destructive method to probe samples. This could be checked by changing significantly the time between sequential acquisitions of two image stacks from twenty to ten minutes. Upon doubling the irradiation time, no significant change in fibrils density could be detected (data not shown).

To better characterize the accuracy of SHG imaging when the fibril volume density is quite low, we focused on the very beginning of the fibrillogenesis for slow kinetic samples (pH = 6.5 ± 0.3). We selected the very beginning of the above time-lapse SHG data, and recorded supplemental SHG images only at early times. For both sets of experimental data, we observed a linear increase of the fibril volume density, as expected for exponential progression at early time. Data were linearly fitted and the inverse of the slope is displayed as the fibrillogenesis rise time at origin (1/r) in Table 1. For fast kinetic samples (pH = 7.5 ± 0.3),

#166900 - $15.00 USD Received 18 Apr 2012; revised 16 May 2012; accepted 16 May 2012; published 21 May 2012

the acquisition duration (about 5 minutes) limited the number of data at the very beginning, so that it was not possible to achieve similar measurements of the onset of fibrillogenesis. Nevertheless, we used the series of data recorded for complete kinetics and calculated the fibrillogenesis rise time as the inverse of the slope at the origin of the exponential fit. We checked for slow kinetic samples that this method provides similar values to linear fitting of the very beginning of the fibrillogenesis (not shown).

Table 1 reports these exponential time constants (τ) and rise time at origin (1/r) for every sample with slow (pH = 6.5 ± 0.3) and fast (pH = 7.5 ± 0.3) kinetics. Overall, Table 1 shows that a good reproducibility is achieved: similar values are obtained at a fixed pH, while significantly different kinetics are measured when comparing samples having different pH. This is clearly seen in Fig. 3(c) that displays the mean exponential time constant for slow kinetics: 405 ± 62 min and for fast kinetics: 54 ± 14 min, and the mean rise time at origin for slow kinetics: 166 ± 35 min and for fast kinetics: 44 ± 12 min. These measurements allow a clear discrimination between the two populations of samples. Further statistical analysis was performed using R software (R development core team, R foundation for statistical computing, version 2.14.1). F-test, with critical value set as 1%, showed that both samples had different variances for whole fibrillogenesis (p = 3.3%) and for fibrillogenesis beginning (p = 3.5%). Then sided two-sample Welsh's t-test for exponential time constants (p = 0.45%) and for fibrillogenesis rise time at origin (p = 0.42%) showed significant differences for slow and fast kinetics.

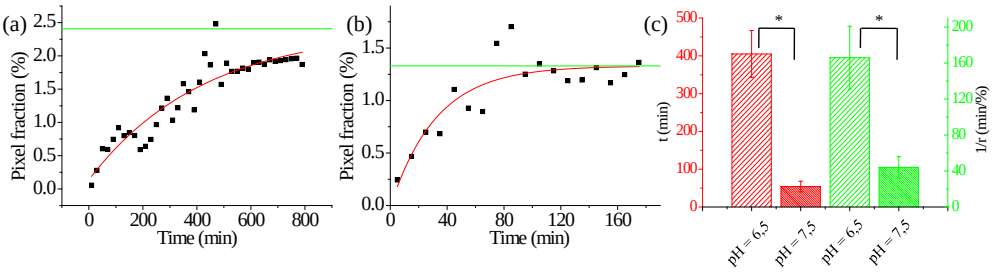

Fig. 3. Quantization of collagen fibrillogenesis using a statistical approach. Fibril volume density (pixel fraction, %) over time (min) for (a) a slow kinetics sample (pH = 6.5 ± 0.3): τ = 352 ± 59 min and (b) a fast kinetics sample (pH = 7.5 ± 0.3): τ = 33 ± 7 min. Black squares and red lines correspond to experimental data and exponential fitting respectively. Green line figures the asymptote of the exponential fit. (c) Statistics over all samples (see Table 1) in every condition. Red and green columns represent respectively the mean time constants and the mean rise time at origin for slow (sparse hatching) and fast (dense hatching) kinetics; error bars represent the standard error of the mean.

Table 1. Time constants obtained for all samples with slow and fast kinetics[a]

Slow kinetics (pH = 6.5 ± 0.3)									
τ (min)	352 ± 59	269 ± 59	543 ± 13	462 ± 124	NA	NA	NA	NA	NA
1/r (min/%)	130 ± 10	82 ± 7	169 ± 29	87 ± 20	105 ± 20	186 ± 10	139 ± 11	169 ± 19	426 ± 42
Fast kinetics (pH = 7.5 ± 0.3)									
τ (min)	39 ± 25	49 ± 17	33 ± 7	93 ± 48					
1/r (min/%)	23 ± 10	72 ± 19	25 ± 5	57 ± 14					

[a]The first row displays time constants (τ) obtained by exponential fitting of fibrils density over time, the second row displays the inverse of the slope at the beginning of fibrillogenesis (1/r). Additional values for fibrillogenesis beginning correspond to five samples studied only during the first two hours. Error intervals correspond to the standard error of fitting parameters. NA: not available.

3.3. Single fibril formation

We also studied the growth of single fibrils. Figure 4 displays time-lapse SHG imaging of a single fibril in a slow kinetic sample (pH = 6.5 ± 0.3). Figure (a) shows projections of SHG image stacks at increasing times after the onset of fibrillogenesis. The growth is more

#166900 - $15.00 USD Received 18 Apr 2012; revised 16 May 2012; accepted 16 May 2012; published 21 May 2012

precisely followed in the corresponding kinetic diagram in Fig. 4(b), where 3D reconstructions of the fibril are tilted and set in the same direction to better evidence the fibril lengthening. It shows that the length of the fibril is well resolved by SHG microscopy and increases significantly with time to reach *ca* 8.7 µm after about 340 minutes. In contrast, the apparent fibril diameter is 1 to 2 pixels that is about the optical resolution, and do not change significantly during fibrillogenesis. It shows that the fibril diameter is always below the optical resolution, in agreement with TEM images. Both length and diameter of the observed fibrils nicely correlate with reported data on the structure of collagen fibrils [5–7]. In addition, Fig. 4(c) displays the kinetics of the fibril formation. It is measured using the pixel fraction density rather than the fibril length, in order to enable comparison to whole sample kinetics. These data show that the fibril growth is characterized by a time constant of 103 ± 18 minutes. Importantly, similar results were obtained when looking at other single fibrils. This time constant is significantly lower than the characteristic time recorded for the whole sample (405 ± 62 minutes). This is not surprising because the fibrillogenesis kinetics over the whole sample is determined not only by the fibrils length but also by the number of new fibrils.

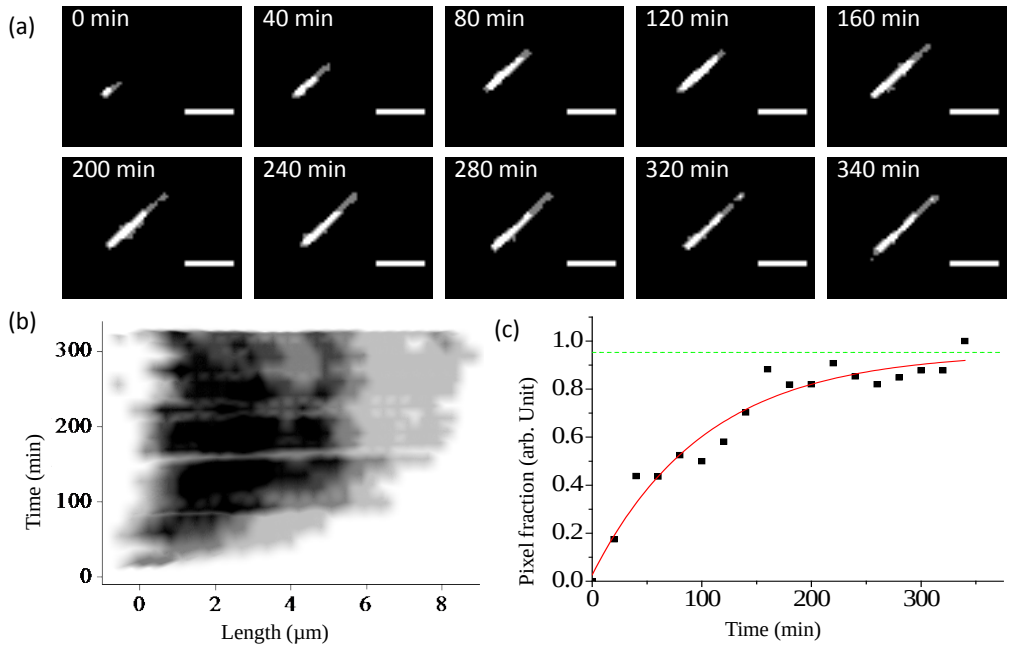

Fig. 4. Kinetics of single fibril growth. (a) SHG images of the same fibril at increasing times after the onset of fibrillogenesis (scale bar: 5µm). (b) Kinetic diagram of the fibril length evolution. (c) Time profile of the area fraction of pixels with significant SHG signal during single fibril formation. The red line corresponds to exponential fitting and provides a time constant of the fibril lengthening of 103 ± 18 min.

4. Discussion

In this work, we used *in situ* time-lapse SHG microscopy to monitor fibrillogenesis of collagen samples. A key advantage of this technique is that it allows continuous non-invasive observation of the assembly of collagen fibrils in solution without any specific preparation. In contrast, when using conventional techniques such as TEM, the fibrillogenesis has to be stopped during image acquisition and one can only record images of different samples dried at different stages of fibril formation [8]. Accordingly, SHG microscopy measures the 3D dynamics of fibrillogenesis with improved reliability and sensitivity. As a proof of concept, we took advantage of the fact that controlled variation of pH allows a significant tuning of the kinetics of fibril formation with a good reproducibility. We obtained significantly different

#166900 - $15.00 USD Received 18 Apr 2012; revised 16 May 2012; accepted 16 May 2012; published 21 May 2012

time constants at pH = 6.5 ± 0.3: around 400 minutes (slow fibrillogenesis), and at pH = 7.5 ± 0.3: around 50 minutes (fast fibrillogenesis). In the former case, the first collagen fibrils could be detected approximately 30 minutes after the induction of fibrillogenesis. TEM micrographs obtained at this stage indicated that the fibril diameter varies typically between 60 and 100 nm. This allowed us to approximate the detection limit of our set-up in this range. SHG microscopy is then sensitive to fibrils with diameters below the optical resolution (360 nm in our set-up in the lateral direction). Compared to TEM that is characterized by very high resolution but limited field of view (few 10 µm), SHG microscopy thus appears as a complementary technique that is sensitive enough to image small collagen fibrils while providing an extended field of view (few 100 µm to 1 mm). This extended field of view is crucial to obtain reliable kinetics since probing fibril formation in larger volume mitigates local singular behavior.

Our results also demonstrate that SHG microscopy enables monitoring the formation of single fibrils in a 3D environment. Recording confocal reflectance images and SHG images of the same collagen sample using the same excitation wavelength and power at focus gives similar sensitivity. Nevertheless, SHG microscopy provides enhanced penetration depth in scattering samples, which should enable the visualization of advanced fibrillogenesis stages in thick tissues. Most importantly, SHG microscopy provides additional information about the supramolecular structure of the collagen fibrils. Indeed, as explained above, SHG probes only tightly aligned collagen molecular structures and scales quadratically with the density of these aligned molecules, while confocal reflectance signals scale linearly with the density of collagen molecules or other entities, including cellular components, regardless of their organization. SHG microscopy therefore ensures that the visualized structures are well-organized fibrils. Moreover, other components like cells may exhibit 2PEF signals, while they generate no SHG signal. Combined SHG/2PEF microscopy therefore appears as a promising technique to simultaneously observe collagen self-assembly and cells behavior in biological samples. It is worth noting that it would require increasing the temperature to typically 37°C that would result in decreased fibril diameter at similar pH, concentration and ionic force conditions. However, these parameters can be optimized to maintain fibrillogenesis and obtain efficient SHG [16,24,25].

The structural specificity of SHG images may be further improved by acquiring polarization-resolved images, which provides a quantitative index of the orientational disorder of collagen distribution within the focal volume [27,28]. Moreover, complete measurement of the SHG tensorial response of collagen fibrils may highlight chiral components as already observed in collagen thin films [23]. Time-lapse experiments should then provide new data about the fibril chirality at various stages of fibrillogenesis. Polarization-resolved SHG imaging however requires longer acquisitions and advanced image processing, and new strategies have yet to be developed to enable monitoring of fast kinetics.

5. Conclusion

In this paper, we used SHG imaging of diluted collagen solutions to monitor and quantify the kinetics of collagen fibrillogenesis. This work illustrates the potential of SHG microscopy for *in situ* 3D imaging of collagen fibrillogenesis with field of view over a few 100 µm. Moreover, this approach allows monitoring the growth of a single fibril using optical microscopy since the sensitivity of SHG microscopy to well-organized fibrils is below the optical resolution. SHG microscopy should therefore provide key insights into the molecular mechanisms of collagen assembly, as well as about the onset of chirality at the supramolecular level. This is a prerequisite to understand biological processes and engineer new biomimetic collagen-based matrices. In this respect, SHG microscopy appears to be a key technique for the rational design and characterization of biomaterials currently developed through a bottom up approach [29].

#166900 - $15.00 USD Received 18 Apr 2012; revised 16 May 2012; accepted 16 May 2012; published 21 May 2012

Acknowledgments

The authors gratefully acknowledge Jérémie Teillon, from the Center for Interdisciplinary Research in Biology—Collège de France, for discussion and experiments using confocal microscopy and Gervaise Mosser and Gaël Latour for fruitful discussions. C. Aimé thanks the ANR-Retour post-doctorant for financial support (ANR-09-RPDOC-023-01).

#166900 - $15.00 USD Received 18 Apr 2012; revised 16 May 2012; accepted 16 May 2012; published 21 May 2012